

ORIGINAL ARTICLE

Truncated UDP-glucuronosyltransferase (UGT) from a Crigler–Najjar syndrome type II patient colocalizes with intact UGT in the endoplasmic reticulum

Masahiro Suzuki¹, Marie Hirata¹, Miho Takagi¹, Taiichi Watanabe¹, Tomohiro Iguchi¹, Kotaro Koiwai^{1,2}, So Maezawa¹ and Osamu Koiwai¹

Mutations in the gene encoding bilirubin UDP-glucuronosyltransferase (UGT1A1) are known to cause Crigler–Najjar syndrome type II (CN-II). We previously encountered a patient with a nonsense mutation (Q331X) on one allele and with no other mutations in the promoter region or other exons, and proposed that CN-II is inherited as a dominant trait due to the formation of a heterologous subunit structure comprised of the altered UGT1A1 gene product (UGT1A1-p.Q331X) and the intact UGT1A1. Here, we investigated the molecular basis of CN-II in this case by expressing UGT1A1-p.Q331X in cells. UGT1A1-p.Q331X overexpressed in *Escherichia coli* or mammalian cells directly bound or associated with intact UGT1A1 *in vitro* or *in vivo*, respectively. Intact UGT1A1 was observed as a dimer using atomic force microscopy. Fluorescent-tagged UGT1A1-p.Q331X and intact UGT1A1 were colocalized in 293T cells, and fluorescence recovery after photobleaching analysis showed that UGT1A1-p.Q331X was retained in the endoplasmic reticulum (ER) without rapid degradation. These findings support the idea that UGT1A1-p.Q331X and UGT1A1 form a dimer and provide an increased mechanistic understanding of CN-II.

Journal of Human Genetics (2014) 59, 158–162; doi:10.1038/jhg.2013.138; published online 9 January 2014

Keywords: Crigler–Najjar syndrome type II; dominant-negative mutation; endoplasmic reticulum; UDP-glucuronosyltransferase; unconjugated hyper-bilirubinemia

INTRODUCTION

Reduced activity of bilirubin UDP-glucuronosyltransferase (UGT1A1) causes three types of unconjugated hyper-bilirubinemia: Crigler–Najjar syndrome type I (CN-I), CN type II (CN-II) and Gilbert's syndrome.¹ Molecular analysis of *UGT1A1* genes from these patients has identified homozygous nonsense or missense mutations and heterozygous missense or deletion mutations.^{2–9} The *UGT1A1* gene from CN-II patients usually contains homozygous missense mutations that result in UGT1A1 enzymatic activity that is only ~10% that of the wild type.¹⁰ However, we previously encountered a unique case of CN-II, in which the *UGT1A1* gene contained a nonsense mutation (Q331X) on one allele, with no additional mutations in the promoter region or other exons.¹¹ Normal UGT1A1 mRNA was synthesized in our patient, suggesting that the CN-II was not caused by the abnormal regulation of *UGT1A1* gene expression.¹¹

UGTs have been reported to form homo- and hetero-dimers *in vitro* and *in vivo*.^{12,13} Rat UGT1A family members can form homo- and hetero-dimers.¹³ Rat UGT1A and the closely related UGT2B1 form a hetero-dimer,¹⁴ as do guinea pig UGT2B1 and UGT2B22.¹⁵ From these facts and our findings described above,

we proposed that in this case CN-II was caused by a dominant-negative mutation of the *UGT1A1* gene, and that the formation of a heterologous subunit structure comprising intact and truncated UGT1A1s decreased the UGT activity.

Here, we further analyzed the truncated UGT1A1 (UGT1A1-p.Q331X) from the CN-II patient (Figure 1) at the molecular level by expressing UGT1A1-p.Q331X in cells. We also showed that intact UGT1A1 forms a dimer by observing UGT1A1 using atomic force microscopy.

MATERIALS AND METHODS

Plasmids

The *UGT1A1* gene (nucleotides 82–1602) and its mutant derived from a CN-II patient with C→T transition at nucleotide 991 (nucleotides 82–991) were subcloned into pPROEX-1 (pPROEX-UGT1A1) or pMAL-c2 (pMAL-c2-UGT330), respectively. A pEGFP-UGT1A1 construct containing a signal peptide upstream of the gene fusion was also generated. UGT1A1-p.Q331X-Venus or UGT1A1-p.Q331X-mKate2 was constructed by replacing the dsRed in dsRed-UGT1A1-p.Q331X with Venus or mKate2, respectively.

¹Department of Applied Biological Science, Faculty of Science and Technology, Tokyo University of Science, Chiba, Japan and ²Department of Biotechnology, Graduate School of Engineering, Nagoya University, Nagoya, Japan
Correspondence: Dr K Koiwai, Department of Applied Biological Science, Faculty of Science and Technology, Tokyo University of Science, Noda, Chiba 278-8510, Japan.
E-mail: koiwai@nubio.nagoya-u.ac.jp

Received 7 July 2013; revised 15 October 2013; accepted 10 December 2013; published online 9 January 2014

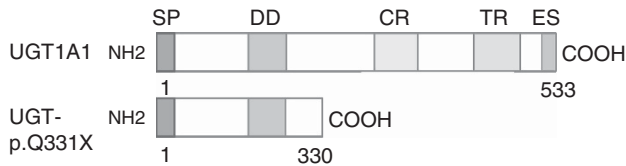


Figure 1 Structural diagram of intact UGT1A1 and UGT1A1-p.Q331X. Most of the UGT1A1 enzyme localizes within the ER lumen except for the carboxyl-terminus, which remains in the cytoplasm. Within the intra-luminal part of the molecule, 152–180 amino acids were proposed to be a trans-membrane region (TR) using the RAOARGOS computer program. In UGT1A1-p.Q331X a C to T transition at nucleotide 991 results in the generation of a premature stop codon. In this mutant, the N-terminal region is normal, containing a signal peptide (SP) and a dimerization domain (DD), but the C-terminal region, which contains the catalytic region (CR), trans-membrane region (TR) and the ER retention signal sequence (ES), is deleted. A full color version of this figure is available at the *Journal of Human Genetics* journal online.

Expression and purification of recombinant UGT1A1

pPROEX-UGT1A1 or pMAL-c2-UGT330 was transformed into *Escherichia coli* BL21 (DE3). Transformed cells were cultured in an LB medium containing 50 $\mu\text{g ml}^{-1}$ ampicillin at 37 °C until the OD600 was 0.6. Protein expression in pMAL-c2-UGT330 or pPROEX-1-UGT1A1 was induced with 0.1 mM IPTG for 3 or 12 h at 22 °C, respectively. The cells were collected and then resuspended in lysis buffer (50 mM Tris-HCl (pH 7.4 at 4 °C), 75 mM NaCl, 0.5% Triton X-100, 5 mM 2-mercaptoethanol, 10% glycerol, 1 $\mu\text{g ml}^{-1}$ PMSF, 1 $\mu\text{g ml}^{-1}$ pepstatin A and 0.5 $\mu\text{g ml}^{-1}$ leupeptin) and then disrupted by sonication (50% cycle power 1.5, 5 s, 5 times). The crude sample was centrifuged at 15 000 r.p.m. and 4 °C for 20 min. Protein concentration was determined by the Bradford method.

Pull-down assay

For the pull-down assay, 300 μg of MBP-UGT1A1 (expressed by pMAL-UGT1A1) or 1000 μg of His-UGT1A1 (expressed by pPROEX-1-UGT1A1) was mixed with His-UGT1A1-p.Q331X (expressed by pPROEX-1-UGT1A1-p.Q331X) for 120 min at 4 °C. Then, 20 μl of Ni^{2+} -agarose (Wako, Osaka, Japan) was added to the mixture, followed by another incubation for 120 min at 4 °C. After incubation, the sample was centrifuged and the pellet was washed with 800 μl of wash buffer (50 mM Tris-HCl (pH 7.4 at 4 °C), 75 mM NaCl, 0.5% Triton X-100, 5 mM 2-mercaptoethanol, 10% glycerol, 30 mM imidazole, 1 $\mu\text{g ml}^{-1}$ PMSF, 1 $\mu\text{g ml}^{-1}$ pepstatin A and 0.5 $\mu\text{g ml}^{-1}$ leupeptin). The proteins bound to the Ni^{2+} -agarose were eluted with SDS sample buffer and analyzed by SDS-PAGE followed by western blotting.

Cell fractionation

293T cells were cultured in 10 cm dishes until 30–50% confluent and then transfected with pEGFP-UGT1A1 and/or pUGT1A1-p.Q331X-mKate2. After 4 h, the medium was changed and the cells were incubated for an additional 48 h. The cells were then collected by centrifugation at 800 r.p.m. for 5 min. The pellet was resuspended in buffer (20 mM HEPES, 0.25 M sucrose) and the cells were disrupted with a Dounce homogenizer. One-third of the sample was kept whole and one-third of the sample was solubilized in 1 ml of the radio-immunoprecipitation buffer (0.05 M Tris-HCl, pH 7.4, 0.15 M NaCl, 0.25% deoxycholic acid, 1% Nonidet P-40, 1 mM EDTA, 1% protease inhibitor mixture) and kept on ice for 60 min. The final third of the sample was centrifuged at 43 000 r.p.m. for 60 min. The nuclear and ER fractions were obtained in the pellet and the cytoplasmic fraction was obtained in the supernatant. The pellet was resuspended in 500 μl of the radio-immunoprecipitation buffer and kept on ice for 1 h.

Immunoblotting was performed according to the protocols of Merck Millipore (Darmstadt, Germany) or Wako. The fluorescent signal was detected with a lumino-imaging analyzer (LAS-1000plus, Fujifilm, Tokyo, Japan).

A polyclonal anti-GFP antibody was produced against the following peptide: NH₂-CPNPFYSYVPRPLSSSDHMTFLQ-COOH. The anti-tubulin antibody was a kind gift from Dr T Arai. Anti-calnexin, anti-Histone H3 and anti-rRFP antibodies were purchased from Medical & Biological Laboratories

(Nagoya, Japan), Sigma-Aldrich Japan (Tokyo, Japan), and Evrogen (Moscow, Russia), respectively. An HRP-labeled mouse monoclonal anti-IgG antibody or rabbit polyclonal anti-IgG antibody was used as a secondary antibody.

Localization of proteins in cells

HEK293T cells were transfected with expression constructs according to the protocols of LipotrustEX (Hokkaido System Science, Sapporo, Japan). After 4 h, the medium was replaced with fresh, phenol-red-free medium and the cells were cultured for an additional 24 h. The medium was removed and the cells were washed with PBS and then fixed with 4% (v/v) paraformaldehyde. The cells were then observed with confocal microscopy (Zeiss LSM5, Carl Zeiss, Jena, Germany), using laser wavelengths of 488, 514 and 543 nm and BP505–530, LP530 and LP560 filters. Image processing was accomplished by the Zen software (Carl Zeiss) and ImageJ.

ER tracker

Cells were washed with HBSS (0.137 mM NaCl, 5.4 mM KCl, 0.25 mM Na₂HPO₄, 0.44 mM KH₂PO₄, 1.3 mM CaCl₂, 1.0 mM MgSO₄ and 4.2 mM NaHCO₃). ER-tracker Red (Life Technologies, Carlsbad, CA, USA) was added to the medium at a final concentration of 100 nM and the cells were cultured for 15 min at 37 °C.

Fluorescence recovery after photobleaching

293T cells expressing EGFP- or Venus-fused proteins were fixed on a glass-bottom dish before photobleaching. The cells were irradiated with a 458- or 488-nm laser and LP505 or LP530 was used as an absorption filter. The gradation and resolution were 12-bit and 128 × 128, respectively, and the Airy unit was two. The bleached area was 2 μm in diameter and there were 200 frames. After 100 scans, the bleaching was initiated. Four scans were carried out during the bleaching. The interval between each frame was 0 s. The fluorescent signal of the entire cell region, the region near the bleaching area and the background were determined over time. The net fluorescence value was obtained by subtracting the background signal from that of the entire cell region or of the region near the bleaching area. The average values before and after bleaching were determined and the relative values between the average fluorescent strength of the region near the bleaching area and of the entire cell region were also calculated. Bleaching efficiency was determined by dividing the average value after bleaching by that before bleaching. The values of the distance and bleach efficiency were entered into the Origin calculation software, and curve-fitting analysis was performed using the bleach constant (K) and practice radius (w) as the variables to fit them to the formula described below. This experiment was performed for 10 cells, and their averages were determined as the final values for K and w . The experiments were performed using both live and fixed cells. The relative fluorescent strength for the region of interest was plotted against time and the fluorescence recovery was calculated. Time (t) and fluorescent strength were entered into Origin and curve-fitting analysis was performed to fit them to the formula described by Axelrod.^{16,17}

AFM analysis

AFM samples were dropped onto a freshly cleaved piece of mica and incubated at room temperature for 10 min. The mica surface was then washed with the Milli Q water. After another 5 min incubation at room temperature, the samples were observed using AFM (Nano-R; Pacific Nanotechnology, Santa Clara, CA, USA) in close contact mode. P-MCU-SICC-0 close contact-mounted cantilevers (Pacific Nanotechnology) were used. AFM images were collected with 512 × 512 pixels under 300 kHz.

RESULTS

Intact UGT1A1 directly binds to UGT1A1-p.Q331X *in vitro*

We first determined that UGT1A1 forms an oligomer by Ni^{2+} pull-down assay. His-tagged UGT1A1 and MBP-tagged UGT1A1 were used as bait and prey, respectively. As shown in Figure 2a, the tagged molecules directly bound each other *in vitro*. We also observed UGT1A1 as a dimer using atomic force microscopy (Figure 2b). We next determined whether UGT1A1 binds to the UGT1A1-p.Q331X

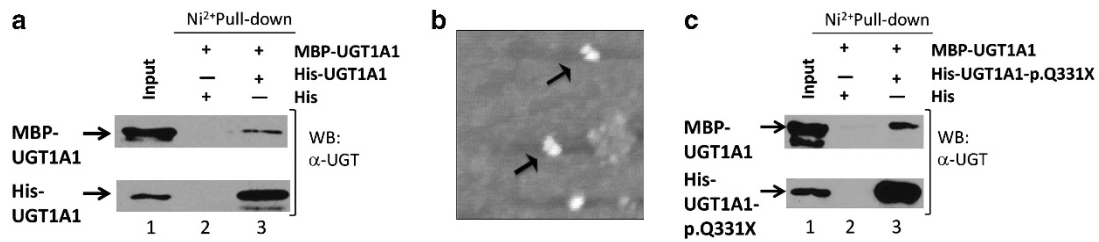


Figure 2 UGT1A1 binds to UGT1A1 or UGT1A1-p.Q331X. (a) UGT1A1 binds to UGT1A1 *in vitro*. Lane 1: His-UGT1A1 and MBP-UGT1A1 expressed in *E. coli* strain BL21 (DE3). Lane 2: SDS eluate of His-bound Ni²⁺ beads following incubation with MBP-UGT1A1. Lane 3: SDS eluate of His-UGT1A1-bound Ni²⁺ beads following incubation with MBP-UGT1A1. (b) UGT1A1 dimerization analysis using AFM. In some of the particles the right-hand side in the dimer was larger than the left-hand side. This configuration may have been caused when the buffer was evaporated by helium gas. (c) UGT1A1 binds to UGT1A1-p.Q331X *in vitro*. Lane 1: His-UGT1A1-p.Q331X and MBP-UGT1A1 expressed in *E. coli* strain BL21 (DE3), Lane 2: SDS eluate of His-bound Ni²⁺ beads following incubation with MBP-UGT1A1, Lane 3: SDS eluate of His-UGT1A1-p.Q331X-bound Ni²⁺ beads following incubation with MBP-UGT1A1. The Ni²⁺ pull-down assay was performed using His-UGT1A1 or His-UGT1A1-p.Q331X as the bait. Eluates were analyzed by SDS-PAGE followed by western blotting using a polyclonal anti-UGT1A1 antibody. A full color version of this figure is available at the *Journal of Human Genetics* journal online.

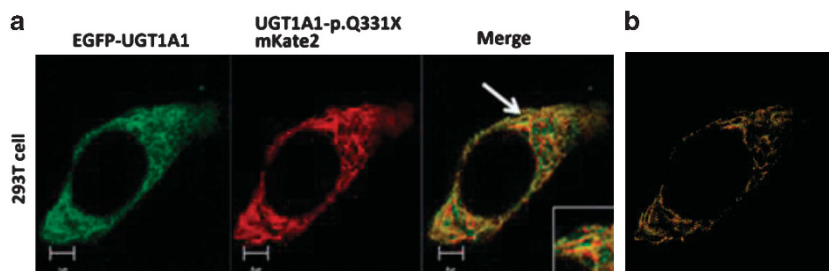


Figure 3 Colocalization of EGFP-UGT1A1 and UGT1A1-p.Q331X-mKate2 in HEK293T cells. (a) Colocalization of EGFP-UGT1A1 and UGT1A1-p.Q331X-mKate2. HEK293T cells were cotransfected with EGFP-UGT1A1 and UGT1A1-p.Q331X-mKate2 expression constructs. EGFP-UGT1A1 and UGT1A1-p.Q331X-mKate2 expressions were observed using fluorescence microscopy. (b) Cut-mask image. The cut-mask area shows only the colocalized pixels in the image by removing the non-overlapping and background pixels using the Zen software.

predicted from the CN-II patient's UGT1A1 DNA sequence. As shown in Figure 2c, His-tagged UGT1A1 directly bound to MBP-tagged UGT1A1-p.Q331X in the *in vitro* Ni²⁺ pull-down assay.

UGT1A1-p.Q331X localizes to the endoplasmic reticulum

UGTs localize to the ER in hepatocytes or kidney cells to detoxify toxic substrates produced within the body. We first observed the localization of EGFP-UGT1A1 and UGT1A1-p.Q331X-mKate by coexpressing them in 293T cells and using fluorescence microscopy. As shown in Figure 3, approximately 60% of the UGT1A1-p.Q331X was colocalized with EGFP-UGT1A1 in a mesh-like structure, strongly suggesting that UGT1A1-p.Q331X interacts with UGT1A1 and is retained in the ER. We also confirmed the localization of UGT1A1 and UGT1A1-p.Q331X in the ER by coexpressing them with ER tracker (data not shown).

To confirm the localization of UGT1A1-p.Q331X in the ER, we determined its distribution by fractionating cell lysates into the cytosol and microsome, which included the nuclei, ER and other organelles. As shown in Figure 4, almost all of the UGT1A1 and UGT1A1-p.Q331X were detected in the microsomal fraction.

UGT1A1 and UGT1A1-p.Q331X are retained in the ER

We next asked whether EGFP-UGT1A1 and UGT1A1-p.Q331X are retained in the ER, using the fluorescence recovery after photobleaching method. As shown in Figure 5, when we used EGFP as a control, all the fluorescence was recovered within 1 s after applying laser radiation to photobleach a small area within the cytoplasm. In contrast, only 50% of the fluorescence was recovered 10 s after

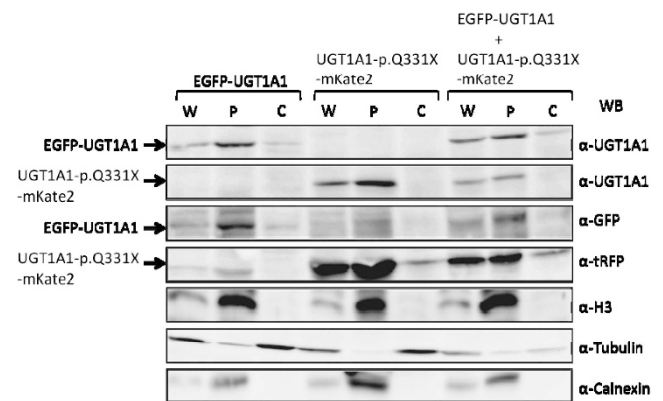


Figure 4 Subcellular localization of EGFP-UGT1A1 and UGT1A1-p.Q331X-mKate2 in 293T cells. Subcellular localization of intact and truncated UGT1A1 determined by fractionating cell lysates from 293T cells expressing EGFP-UGT1A1 or UGT1A1-p.Q331X-mKate2, or both. Whole-cell extracts (W), pellets (P) and soluble cytosolic fractions (C) were analyzed using anti-UGT1A1, anti-GFP or anti-tRFP antibodies. Anti-H3, anti-Calnexin and anti-Tubulin were used as positive control markers for the microsomal and cytosolic fractions.

photobleaching when using EGFP-UGT1A1. The fluorescence after photobleaching Venus-tagged UGT1A1-p.Q331X was also more slowly recovered when compared with the control. The diffusion constants of EGFP, EGFP-UGT1A1 and Venus-tagged UGT1A1-p.Q331X were 0.73, 0.078 and 0.48 $\mu\text{m}^2\text{s}^{-1}$, respectively. The average proportion of EGFP-UGT1A1 and Venus-tagged UGT1A1-p.Q331X

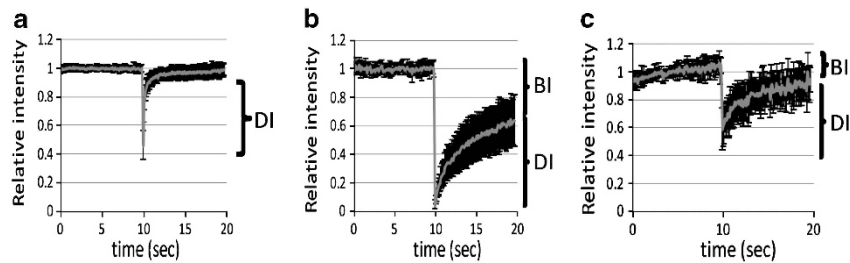


Figure 5 Fluorescence photobleaching of EGFP, EGFP-UGT1A1 and UGT1A1-p.Q331X-Venus. HEK293T cells expressing EGFP (a), EGFP-UGT1A1 (b) or UGT1A1-p.Q331X-Venus (c) were subjected to photobleaching and the fluorescence recovery after photobleaching recoveries were determined. Figures show the mobility of the EGFP, EGFP-UGT1A1 or UGT1A1-p.Q331X-Venus molecules. Images were captured using an LSM5 33 EXCITER confocal microscope (Carl Zeiss). Excitation was performed at 488 (514) nm to visualize EGFP (Venus) using LP505 (530) nm emission filters. Fluorescence recovery after photobleaching was performed using the region of interest, 2 μ m in diameter, and four bleaching iterations. Graphic imaging was processed with the Zen software. A full color version of this figure is available at the *Journal of Human Genetics* journal online.

bound to the ER membrane was 72% and 42%, respectively. These results indicate that EGFP-UGT1A1 is not diffusible and is retained in the ER, and that UGT1A1-p.Q331X is also retained in the ER.

DISCUSSION

We previously encountered a CN-II patient with a heterozygous nonsense mutation and proposed that the manifestation of CN-II was caused by a dominant-negative mechanism, as UGT1A1 has been shown to form an oligomer.¹¹ Here we further analyzed the UGT1A1-p.Q331X derived from this patient and found that it colocalized with UGT1A1 in the ER. We also demonstrated for the first time that UGT1A1 is a dimer using AFM.

UGT1A1 was initially suspected to form a homo-tetramer based on UV-radiation inactivation analysis.¹⁸ We previously expressed the truncated and intact UGT1A1 in COS 7 cells and found that the resulting UGT had 6% of the original wild-type UGT activity.¹¹ From these results, we proposed that a hetero-oligomer containing both intact and truncated UGT1A1 functions as a dominant-negative mutant resulting in reduced UGT activity. Our present observation using AFM showed that UGT1A1 formed a dimer under our experimental conditions. Abnormal proteins synthesized within the ER are usually degraded after their detection by the endoplasmic reticulum-associated protein degradation system in the ER. The Gunn rat carries a homozygous nonsense mutation in the C-terminal region resulting in a truncated UGT1A1, which lacks 126 amino-acid residues. Although the half-life of normal UGT1A1 is 10 h, that of the isoform present in the Gunn rat is 50 min, suggesting that the mutant UGT1A1 is rapidly degraded by the endoplasmic reticulum-associated protein degradation system.¹⁹ In contrast, the UGT1A1-p.Q331X in the present study appeared to exist in the ER without undergoing degradation. Observations using fluorescence microscopy showed that UGT1A1-p.Q331X colocalized with the intact UGT1A1 in the ER, strongly supporting our hypothesis that CN-II results from a dominant-negative effect caused by the formation of a complex of intact UGT1A1 and UGT1A1-p.Q331X in the ER.

Proteins present within/on the ER generally have an ER retention signal of KXXXX or KKXX at the carboxyl terminal end. The ER retention signal is no longer expressed in the truncated UGT1A1-p.Q331X, indicating that this mutant would not be expected to localize to the ER. However, UGT1A1-p.Q331X was found in the microsomal fraction using subcellular fractionation, suggesting that UGT1A1-p.Q331X is still localized in the ER. When we expressed UGT1A1-p.Q331X solely in 293T cells, in which UGT1A1 is scarcely expressed, it was observed in the ER (Supplementary Figure 1), thus confirming that the ER retention signal was not required for

UGT1A1-p.Q331X to localize to the ER. These findings collectively indicate that UGT1A1-p.Q331X exists in the ER as a hetero-oligomer with an intact UGT1A1 and/or as a homo-oligomer. Recently, UGT1A1 was found to have two isoforms (isoforms 1 and 2) that form a hetero-oligomer with reduced UGT activity.²⁰ Isoform 2 lacks the C-terminal region, similar to our UGT1A1-p.Q331X, supporting our hypothesis that CN-II is caused by a dominant-negative mutation.

The findings presented here strongly suggest that UGT1A1-p.Q331X localizes to the ER as a heterologous complex of intact UGT1A1 and UGT1A1-p.Q331X, resulting in a dominant-negative suppression of the UGT activity.

- 1 Tukey, R. H. & Strassburg, C. P. Human UDP-glucuronosyltransferases: metabolism, expression, and disease. *Annu. Rev. Pharmacol. Toxicol.* **40**, 581–616 (2000).
- 2 Berk, J. E. Bockus Lecture: World Congress of Gastroenterology, Los Angeles, CA–October 3, 1994. The management of acute pancreatitis: a critical assessment as Dr Bockus would have wished. *Am. J. Gastroenterol.* **90**, 696–703 (1995).
- 3 Aono, S., Yamada, Y., Keino, H., Sasaoka, Y., Nakagawa, T., Onishi, S. *et al.* A new type of defect in the gene for bilirubin uridine 5'-diphosphate-glucuronosyltransferase in a patient with Crigler-Najjar syndrome type I. *Pediatr. Res.* **35**, 629–632 (1994).
- 4 Yamamoto, K., Soeda, Y., Kamisako, T., Hosaka, H., Fukano, M., Sato, H. *et al.* Analysis of bilirubin uridine 5'-diphosphate (UDP)-glucuronosyltransferase gene mutations in seven patients with Crigler-Najjar syndrome type II. *J. Hum. Genet.* **43**, 111–114 (1998).
- 5 Maruo, Y., Poon, K. K., Ito, M., Iwai, M., Takahashi, H., Mori, A. *et al.* Co-occurrence of three different mutations in the bilirubin UDP-glucuronosyltransferase gene in a Chinese family with Crigler-Najjar syndrome type I and Gilbert's syndrome. *Clin. Genet.* **64**, 420–423 (2003).
- 6 Petit, F., Gajdos, V., Capel, L., Parisot, F., Myara, A., Francoual, J. *et al.* Crigler-Najjar type II syndrome may result from several types and combinations of mutations in the UGT1A1 gene. *Clin. Genet.* **69**, 525–527 (2006).
- 7 Sneitz, N., Bakker, C. T., de Knegt, R. J., Halley, D. J., Finel, M. & Bosma, P. J. Crigler-Najjar syndrome in The Netherlands: identification of four novel UGT1A1 alleles, genotype-phenotype correlation and functional analysis of 10 missense mutants. *Hum. Mutat.* **31**, 52–59 (2010).
- 8 Aono, S., Yamada, Y., Keino, H., Hanada, N., Nakagawa, T., Sasaoka, Y. *et al.* Identification of defect in the genes for bilirubin UDP-glucuronosyl-transferase in a patient with Crigler-Najjar syndrome type II. *Biochem. Biophys. Res. Commun.* **197**, 1239–1244 (1993).
- 9 Koizumi, O., Nishizawa, M., Hasada, K., Aono, S., Adachi, Y., Mamiya, N. *et al.* Gilbert's syndrome is caused by a heterozygous missense mutation in the gene for bilirubin UDP-glucuronosyltransferase. *Hum. Mol. Genet.* **4**, 1183–1186 (1995).
- 10 Arias, I. M., Gartner, L. M., Cohen, M., Ezzer, J. B. & Levi, A. J. Chronic nonhemolytic unconjugated hyperbilirubinemia with glucuronyl transferase deficiency. Clinical, biochemical, pharmacologic and genetic evidence for heterogeneity. *Am. J. Med.* **47**, 395–409 (1969).
- 11 Koizumi, O., Aono, S., Adachi, Y., Kamisako, T., Yasui, Y., Nishizawa, M. *et al.* Crigler-Najjar syndrome type II is inherited both as a dominant and as a recessive trait. *Hum. Mol. Genet.* **5**, 645–647 (1996).
- 12 Ghosh, S. S., Sappal, B. S., Kalpana, G. V., Lee, S. W., Chowdhury, J. R. & Chowdhury, N. R. Homodimerization of human bilirubin-uridine-diphosphoglucuronate glucuronosyltransferase-1 (UGT1A1) and its functional implications. *J. Biol. Chem.* **276**, 42108–42115 (2001).

- 13 Operana, T. N. & Tukey, R. H. Oligomerization of the UDP-glucuronosyltransferase 1A proteins: homo- and heterodimerization analysis by fluorescence resonance energy transfer and co-immunoprecipitation. *J. Biol. Chem.* **282**, 4821–4829 (2007).
- 14 Ikushiro, S., Emi, Y. & Iyanagi, T. Protein–protein interactions between UDP-glucuronosyltransferase isozymes in rat hepatic microsomes. *Biochemistry* **36**, 7154–7161 (1997).
- 15 Ishii, Y., Nurrochmad, A. & Yamada, H. Modulation of UDP-glucuronosyltransferase activity by endogenous compounds. *Drug. Metab. Pharmacokinet.* **25**, 134–148 (2010).
- 16 Axelrod, D., Koppel, D. E., Schlessinger, J., Elson, E. & Webb, W. W. Mobility measurement by analysis of fluorescence photobleaching recovery kinetics. *Biophys. J.* **16**, 1055–1069 (1976).
- 17 Sprague, B. L. & McNally, J. G. FRAP analysis of binding: proper and fitting. *Trends Cell Biol.* **15**, 84–91 (2005).
- 18 Peters, W. H., Jansen, P. L. & Nauta, H. The molecular weights of UDP-glucuronosyltransferase determined with radiation-inactivation analysis. A molecular model of bilirubin UDP-glucuronosyltransferase. *J. Biol. Chem.* **259**, 11701–11705 (1984).
- 19 Emi, Y., Omura, S., Ikushiro, S. & Iyanagi, T. Accelerated degradation of mislocalized UDP-glucuronosyltransferase family 1 (UGT1) proteins in Gunn rat hepatocytes. *Arch. Biochem. Biophys.* **405**, 163–169 (2002).
- 20 Levesque, E., Girard, H., Journault, K., Lepine, J. & Guillemette, C. Regulation of the UGT1A1 bilirubin-conjugating pathway: role of a new splicing event at the UGT1A locus. *Hepatology* **45**, 128–138 (2007).



This work is licensed under a Creative Commons Attribution-NonCommercial-NoDerivs 3.0 Unported License. To view a copy of this license, visit <http://creativecommons.org/licenses/by-nc-nd/3.0/>

Supplementary Information accompanies the paper on Journal of Human Genetics website (<http://www.nature.com/jhg>)